Enhancing micro-Doppler classification using Superlet based time-frequency distribution

Luca Mignone*, Christos Ilioudis[†],

Carmine Clemente,[†] and Silvia Ullo*

* Universia' degli Studi del Sannio, Benevento, Italy.

[†] University of Strathclyde, Glasgow, UK.

Abstract

Classical time-frequency distributions, as the Short Time Fourier Transform (STFT) or the Continuous Wavelet Transform (CWT), aim to enhance either the resolution in time or frequency, or attempt to strike a balance between the two. In this paper, we demonstrate how a super resolution technique, the Superlet based time frequency distribution, named Superlet Transform (SLT), can boost the performance of existing classification algorithms relying on information extraction from the micro-Doppler signature. SLT is applied to provide a time-frequency distribution with finer resolutions that would boost the performance of micro-Doppler classification approaches based on time-frequency distributions (TFDs). This work shows the effectiveness of the integration of SLT in the processing pipeline with verification on real radar data.

Index Terms

Time-frequency representation, micro-Doppler, Superlet Transform, human motion recognition.

I. INTRODUCTION

In radars when besides the main target body other parts display an extra motion an effect called micro-Doppler (mD) is generated, introducing an intricate frequency modulation creating sidebands around the main Doppler shift [1]. The time-frequency (TF) representation of this effect is called mD signature and is widely used to extract additional insights about the target and to perform recognition tasks [2]. In the last few decades, the interest in mD has grown significantly, in part, due to the improvement and integration of FPGAs, which have enabled TF analysis tools to be exploited in real-time with applications in a wide range of fields including defence, security, biomedical signal processing, assisting living and industry 4.0 [3]-[4]-[5]-[6].

The classification of targets using their mD signatures has become more and more popular recently. MD modulations carry a signature that can be utilized to identify the target. Target classification using those signatures has received a lot of attention in the radio frequency (RF) regime, particularly in radar-related applications [7], [8], [9], [10].

The activities that can be classified are numerous, depending on the target type, and these may include object and human identification in different environments and under different weather conditions, just to give some examples

August 15, 2023

[11]-[12]-[13]-[14]-[15]. To distinguish the answers from various targets, it is important to obtain a synthetic feature that preserves the original signal's attribute. Algorithms for extracting signatures have been created, tested with real data, and produced characteristics that result in highly accurate classification outcomes [16]. While not always necessary, the most used domain to analyse and exploit the mD information is the "signature" domain, relying on TF representation of the mD signal. Classical TFDs, in particular the atomic ones, optimize either temporal or frequency resolution, or find a sub-optimal trade-off among these quantities. To overcome this trade-off a number of alternative approaches have been proposed in the literature when dealing with micro-Doppler analysis, for example in [17] the Reassigned Joint time-frequency transform was investigated to represent micro-Doppler signatures from humans, demonstrating improvements in the capability to discriminate specific components when compared with the spectrogram. The reassigned spectrogram approach was also investigated in [18], in which Hermite functions were employed to enhance the Rényi entropy of the resulting time-frequency distribution. Another example was presented in [19], introducing a 2D minimum variance time-frequency distribution to achieve enhanced resolution. In this case, the performance was qualitatively assessed on real radar data from humans and helicopters.

In the field of neuroscience, to overcome the time-frequency resolution trade-off, a novel technique was introduced in [20] with application to neuroscience. Its major advantage is the capability to achieve a "super-resolution" TF distribution of a signal, thus allowing richer information to be extracted.

In this paper, we demonstrate how the Superlet based TF distribution can benefit also micro-Doppler classification tasks as a replacement to the Specprogram. The primary objective of this work's content is, therefore, showing how the use of this new TF distribution can boost the performance of existing algorithms relying on information extraction from the mD signature. For the remaining part, Section II describes the Superlet based time-frequency distribution (TFD) while Section III details the dataset used in this paper and shows the differences between the TFDs obtained with the Superlet approach compared with the spectrogram. Section IV presents the integration of the transformed distribution, as from Section II, within the TF resolution-dependent classification approach and the obtained outcomes. Conclusions end this manuscript.

II. SUPERLET TRANSFORM

In [20], a new TF super-resolution spectral estimator is introduced, called Superlet, with application to neuroscience. A well known strategy in signal analysis involves the use of several windows to compute spectrograms and merge multiple estimates [21], [22]. The approach in [20] exploits this concept, while several wavelets are utilized, instead of just one, to enhance the detection of localized TF components, and achieve a "super-resolution". Among the various types of wavelets, the Morlet is used [23]. The Morlet wavelet is a type of wave that is shaped like a plane one and is multiplied by an envelope that has a Gaussian distribution defined as in 1

$$\psi_{f,p}(t) = \frac{1}{B_p\sqrt{2\pi}} e^{-\frac{t^2}{2B_p^2}} e^{j2\pi ft} \tag{1}$$

with

$$B_p = \frac{p}{k_{sd}f} \tag{2}$$

the time spread parameter, k_{sd} standing for k times the standard deviation of the Gaussian, p the number of cycles, and f the wavelet's center frequency [23].

The spread parameter B_p controls the variance of the wavelet and depends on f^{-1}. Thus, if the B_p decreases, the energy is distributed across a broader range of frequencies, while the opposite is true if the B_p is larger. Concerning the Morlet wavelet, although not exposing compact support, it offers various benefits, such as the optimal concentration of joint time-frequency; a higher number of cycles when the value of the spread parameter is high, i.e. a wider time response, yet, with the disadvantage of narrower bandwidth.

A normalization of the wavelet is made in [20], to permit the measurement of the instantaneous power by the wavelet at scale, without being dependent on the frequency. In the identification of wavelet ridges the above form has been extensively applied. Indeed, with this normalization, self-similar events across scales become better detectable by the wavelet: if they exhibit similar shape and maximum value, their representation shows the same intensity levels, regardless of any scaling (compression or dilation) they undergo.

By using a predetermined value of cycles for the Morlet wavelet a constant time resolution is obtained, however this affects the frequency resolution due to the increase of the central frequency of the wavelet. On the contrary, by increasing the number of cycles the frequency resolution is improved while losing in terms of time resolution. To overcome this issue short wavelets, with small number of cycles and low time spread parameter, providing high temporal resolution are combined with longer wavelets, with larger number of cycles, that provide higher frequency resolution.

A set of wavelets is referred to as superlet (SL) and is described by the equation:

$$SL_{f,o} = \{\psi_{f,p} | p = p_1, p_2, ..., p_0\} \tag{3}$$

where f is a fixed central frequency, and for every wavelet, p_1, p_2,...p_0 represent the cycles' number, with the SL order indicated with o. Similar to the CWT, the SL transform (SLT) is calculated, with the exception that SLs are used in place of wavelets. For clarity, choosing an SLT order of 1 would be equivalent to working with a CWT. Another thing to consider are the Adaptive SLs (ASLs), which, to account for the widening bandwidth of the wavelet at higher frequencies, modify their order to align it with the central frequency: low order is used for low-frequency estimation, then it is incremented accordingly. This is formalized as follows:

$$ASL_f = SL_{f,o} | o = a(f) \tag{4}$$

where $a(f)$ is an integer-value directly related to the central frequency, meaning that as the central frequency increases, so does this value. The order is obtainable as a linearly variable:

$$a(f) = o_{min} + [(o_{max} - o_{min}) \cdot \frac{f - f_{min}}{f_{max} - f_{min}}] \tag{5}$$

with o_{max} the order corresponding to the largest central frequency (f_{max}), and o_{min} to the smallest, and $[(\cdot)]$ is the nearest integer (round) operator.

An example testifying the effectiveness of ASL and ASL Transform (ASLT) is given in [20], where the STFT appeared to be unable to separate time and frequency, even using a window for a sub-optimal trade-off; the CWT showed better frequency resolution only at low frequencies, while the ASLs, on the other hand, showed both in

time and in frequency domains better resolution throughout the spectrum. Time resolution is penalized at low frequencies, but it is possible to achieve greater resolution in time by decreasing p_1 and compensate for the poor resolution in frequency by increasing orders. The evidence of SLT effectiveness is also shown in this case by taking electroencephalography images as examples.

A drawback of ASLT regards the issue related to the discrete jumps as the frequency increases, resulting into a "banding" in the representation, mainly due to the fact that the order is an integer number. A solution to this problem is offered by the Fractional Superlets (FSLs) [24]. Thanks to a fractional number for the order, their representations exhibit high resolution and provide a smooth spectrum, surpassing those created with discrete ASLs.

In order to define the FSL Transform (FSLT), we start from the ASLT notation given in [24] highlighting the changes. The equations:

$$\psi_m(\omega_m, p_m; t) = \frac{1}{\sigma_m \sqrt{2\pi}} e^{\frac{1}{2}[\frac{t}{\sigma_m}]^2} e^{j\omega_m t} \tag{6}$$

$$\sigma_m = \frac{2\pi p_m}{5} \tag{7}$$

show how the mother wavelet depends on two parameters: the first one p_m, fixing the cycles' number equal to the central frequency ω_m, that represents the second parameter. The arbitrary nature of ω_m allows to set its value to 1 for simplicity and without affecting the results. Given all the above, the child wavelets are then represented as:

$$\psi(p_m; t, \omega) = \frac{5\omega}{p_m (2\pi)^{\frac{3}{2}}} e^{-\frac{1}{2}[\frac{5\omega t}{2\pi p_m}]^2} e^{j\omega t} \tag{8}$$

and considering this formula, the SLT is given by:

$$SLT_{x,p_1,o}(t,\omega) = \prod_{i=1}^{o} [R_x(p_1 \cdot i; t, \omega)]^{\frac{1}{o}} \tag{9}$$

where a convolution between the signal x and the generic wavelet with p_i cycles generates $R_x(p_i; t, \omega)$:

$$R_x(p_i; t, \omega) = \sqrt{2} \int_{-\infty}^{+\infty} x(\tau) \psi(p_i; \tau - t, \omega) d\tau \tag{10}$$

With the definition of SLT as given by formula 9, the orders are defined as in equation 5. This creates the "banding" effect as introduced before due to the discrete steps.

The FSLs come to help. They can work with fractional order o_f in accordance with equation (11):

$$o_f = o_i + \alpha \tag{11}$$

where o_i is an integer ≥ 1 while $\alpha \in [0, 1)$.

FSLT is calculated through the equation:

$$FSLT(t,\omega) = [R_x(p_1[o_i + 1]; t, \omega)^{\alpha} \prod_{i=1}^{o_i} R_x(p_1 \cdot i; t, \omega)]^{\frac{1}{o_f}} \tag{12}$$

where the fractional part of o_f is used to calculate the weighted geometric mean. If the value of α is zero, then FSLT is equivalent to SLT. By utilizing SLTs, the multiscale TF representations are significantly improved, which addresses the issue of low frequency resolution that is present in CWT.

Unlike STFT, which uses absolute time windows [25], SLs are based on oscillation cycles, and it is possible to select them regardless of the representation frequency range. Simplicity and straightforward implementation represent one of the main advantages of SLs: choosing the two parameters p_1 and o is relatively easy, taking into account that the basic wavelet rules the time resolution, and the frequency sharpness of the representation is determined instead by the order value.

In order to show the benefits in terms of resolution with SL based approach for signals with time-frequency characteristics typical of micro-Doppler signals, we present the results obtained when simulating a simple signal with periodic frequency modulation, of the form $x(t) = A_0 e^{j A_1 \cos(2\pi f_{mod}t)}$, with $A_0 = 1$, $A_1 = 100$, and $f_{mod} = 1$ and t is the time. Both the SLT and the spectrogram are computed for the signal $x(t)$, the SLT is obtained using p_1=1, $o = [1, 30]$ and 512 DFT bins, while the spectrogram is computed with the same number of DFT bins, a 256 samples hamming windows and 93% overlap. The resulting time-frequency distributions are shown in Figures 1 (a) and (b), on both time-frequency distributions the column and row analysed in Figures 1 (c) and (d) are also shown (pink line for the frequency cut and green line for the cut in time). From both the time-frequency distributions and the cuts it is possible to appreciate the improvement in resolution and sidelobe reduction. In particular, in Figure 1 - (c) the frequency cut shows how the superlet (with the used settings) reduces significantly the sidelobes generated by the spill-over of other frequency component in a given time-window of the STFT, moreover the improvement in resolution is time is significant in Figure 1-(d).

III. EXPERIMENTAL SETUP AND DATASET

The objective of this study is to test whether the Superlet technique enhances the capabilities of TF distribution mD-based algorithms. In order to assess this capability, using a Frequency Modulated Continues Wave (FMCW) V-MD3 from RFbeam Microwave GmbH [26], a dataset of measurements of humans performing different daily activities has been generated.

The generated dataset was gathered with the support of five volunteers, asked to perform 20 repetitions of five actions: walking, sitting down, standing up, picking up an object and drinking water. Relevant information about the five subjects are reported in table I. A measurement area was then set up (Figure 2) in which the sensor could unobstructedly detect the movement of the targets.

Subject ID	Age	Height [cm]	Dominant Hand	Gender
1	24	178	right hand	male
2	27	167	right hand	male
3	23	177	right hand	male
4	29	164	right hand	female
5	25	185	right hand	male

TABLE I: *Volunteers informations.*

For each activity and participant, 20×5 seconds recordings were gathered, for the non-walking activities the subject was positioned 2m away from the radar, while for the waking activities the targets were moving between a distance of 0.3 and 3.9m from the radar.
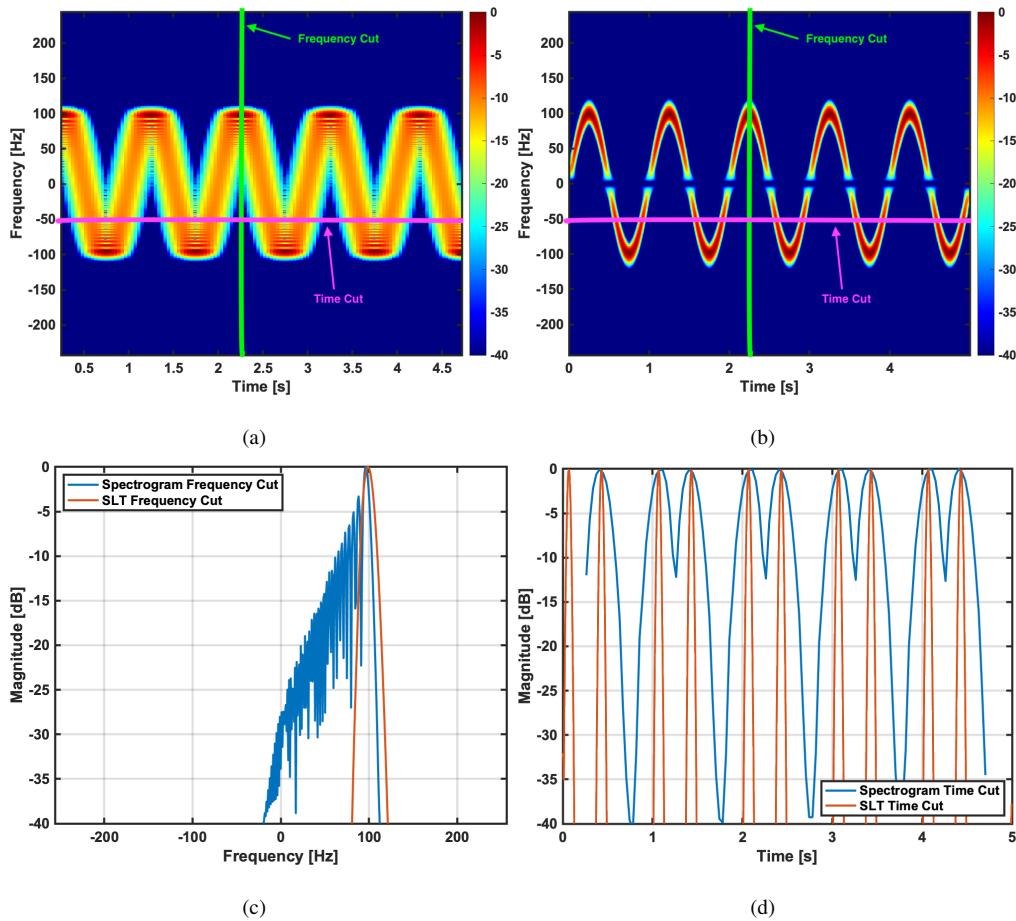
Fig. 1: *a) Spectrogram of the simulated signal $x(t)$, b) its SLT, c) cut in frequency, d) cut in time.*

IV. FEATURE EXTRACTION AND RESULTS

To derive the mD signature for each acquisition, the TF distribution of the complex-valued time series is calculated, extracted by averaging the range bins between 0.3 and 3.9m from the radar. In addition, a clutter removal stage is included before the computation of the TFD in order to remove stationary clutter return. To perform this task a FIR a high pass (HP) filter has been used in our analysis with 10 Hz as cutoff frequency, pass frequency of 15 Hz and order 1242. In Figure 3 the spectrograms and the SLTs obtained for the five activities are shown. The top rows show the spectrogram computed using a 256 samples-long Hamming window and 512 DFT bins, while the bottom row shows the SLTs obtained using p_1=1, $o = [5, 40]$ and 512 DFT bins. From the figure it can be appreciated how the SLTs provide finer resolution in both time and frequency, thus suggesting that finer details could be captured by ad-hoc or automated feature extraction strategies.

As the scope of this paper is to show that the use of SLT has the potential to enhance micro-Doppler classification, in this work a simple but effective feature extraction strategy has been selected. The main reason for this selection is that we want to highlight the potential gain in performance deriving from the use of the SLT rather than defining the
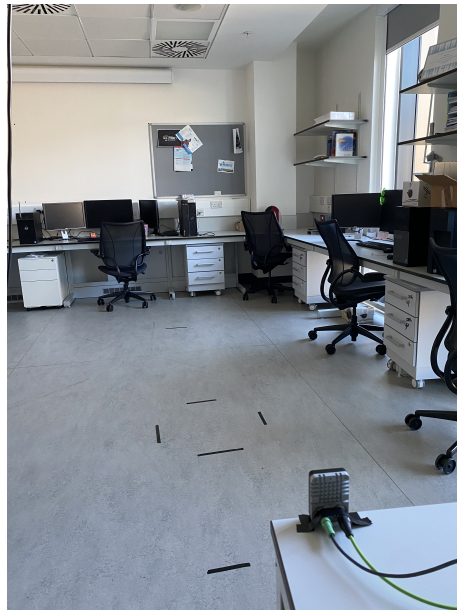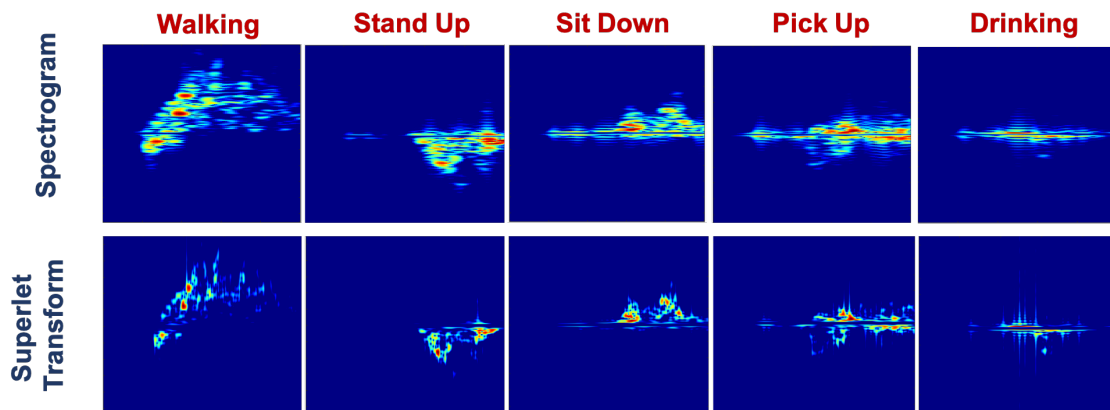
Fig. 2: *Measurement area.*

Fig. 3: *Spectrograms (top) and Superlet Transforms (bottom) of the five activities.*

most performing or reliable feature extraction strategy[1]. For this reason, the feature extraction approach presented in [16] is used in this work, and as feature is considered the mean frequency profile (MFP) computed through equation (13), by averaging over the M time instants the absolute TFD as a function of the frequency. $MFP(\nu) \in R^L$, with L the number of frequency points, and is evaluated for both the spectrogram and the SLT, to allow comparisons.

$$MFP(\nu) = \frac{1}{M} \sum_{m=1}^{M} |TFD(\nu, m)| \tag{13}$$

Given its straightforward formulation, it is intuitive to expect that if the TFD is richer in detail, a more discriminative MFP can be obtained.

---

[1]These aspects are subject of ongoing and future work.

Figure 4 shows the spectrogram MFPs for the five activities for one of the twenty repetitions. The first figure shows the walk of a subject approaching the sensor, as can easily be seen from the negative frequency position of the peaks, while the second shows a subject walking away (peaks at positive frequencies). The next two figures, respectively, show a subject sitting, as attested by positive frequencies peaks (by sitting there is a movement of the torso away from the sensor) and standing up, as attested by negative frequencies peaks (by standing up there is a movement of the torso closer to the sensor). A special case concerns drinking and picking up an object, as both movements show approximately the same frequency pattern, but in the case of drinking, the peak has a smaller width as the movement is only relative to the arm and not to the body. For comparison, Figure 5 sketches the MFPs of the SLTs, and two main characteristics can be identified: 1) the dynamic of the MFP of the SLT is much larger compared to that obtained from the spectrogram, confirming that in the SLT the energy distribution of the TFD is more concentrated; 2) the SLT MFP is smoother and the main Doppler characteristics can be identified clearly.
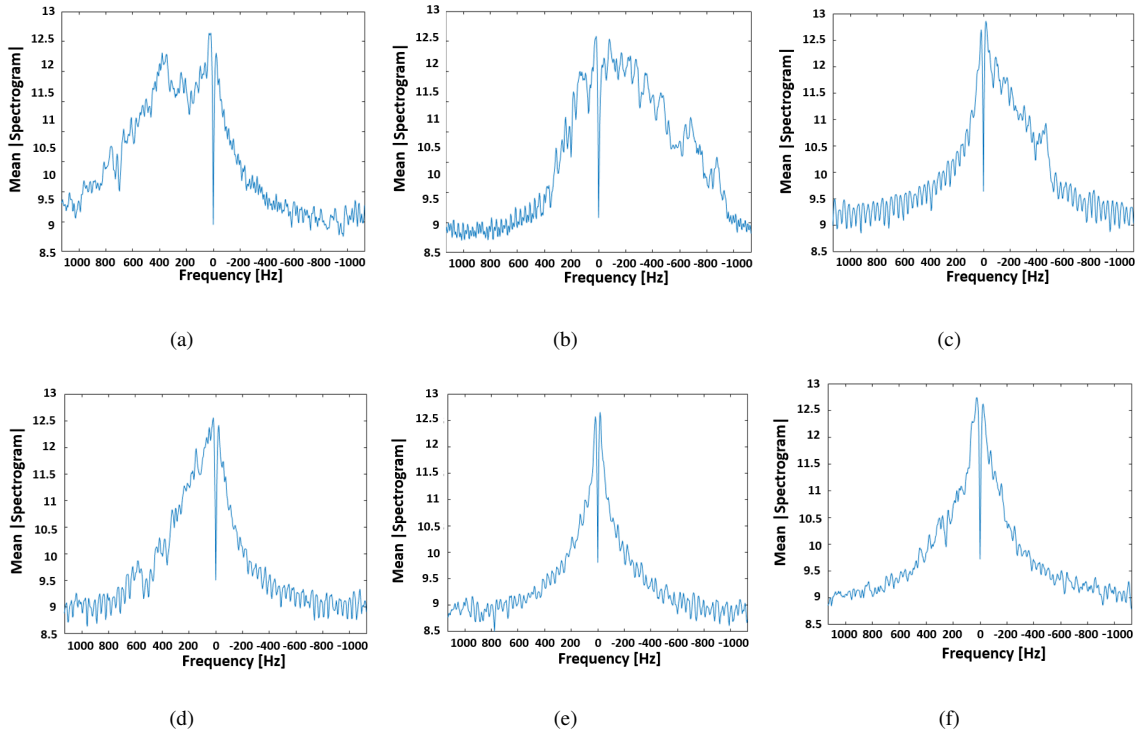

Fig. 4: *MFP of spectrograms respectively for a) walking approaching the sensor, b) receding the sensor, c) sitting, d) standing up, e) drinking, f) picking up an object.*

As in [16], the final step in the feature extraction approach entails scaling the feature vectors F by normalizing them with a zero mean μ and unit variance range σ^2.

$$\hat{F} = \frac{F - \mu}{\sigma} \tag{14}$$

Finally, a k-NN classifier is selected to assess the classification performance. This specific classifier is selected for its simplicity and allows quantifying the performance differences deriving from the "quality" of the features
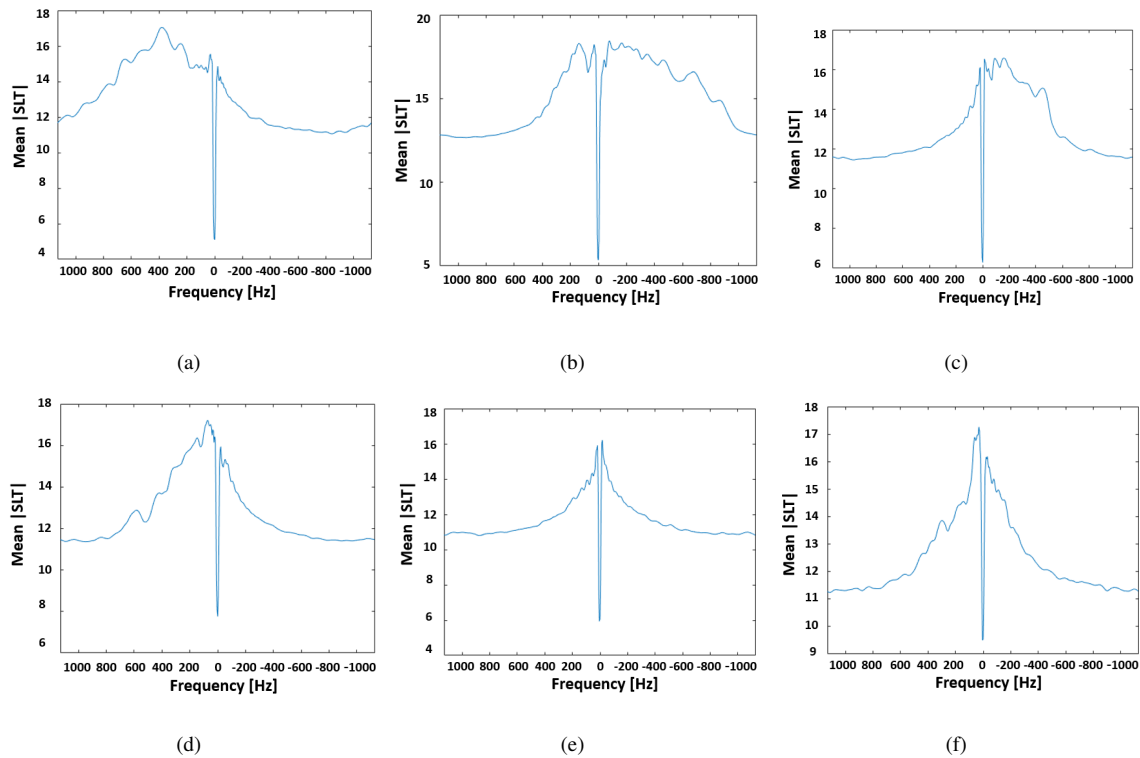
Fig. 5: *MFP of SLTs respectively for a) walking approaching the sensor, b) receding the sensor, c) sitting, d) standing up, e) drinking, f) picking up an object.*

fed only. The analysis is conducted by randomizing the test and training sets 100 times and using a 70/30 splitting percentage between training and testing as commonly done [27].

Considering the spectrograms obtained with a 256-length Hamming window, a 93% overlap, and 512 DFT points, using five neighbors in the classifier $k = 5$, an average correct classification percentage of 94.89% over 100 tests is obtained. Considering the Superlets obtained with the same frequency resolution, i.e. using the same number of frequency points, a higher classification accuracy is obtained: 97.89%. This denotes the effectiveness of the SLT in classification when it has a finer temporal resolution.

The spectrogram-based approach's average confusion matrix is represented in Figure 6. The evidence indicates that classification errors are made specifically when distinguishing between 4 and 5 classes (someone picking up an object and someone drinking). The explanation for this error can be found in the similar MFPs of these two activities, as shown in Figure 4. This issue appears to be mitigated when using the Superlet, as shown in Figure 7. The latter confusion matrix shows also how the SLT based approach outperforms the Spectrogram one for each individual class, with the exception of class 5. The color coding on the confusion matrices shows in green the cases in which one approach outperforms the other while in red are highlighted the cases in which the approach has worse performance.

Finally, to assess how noise affects the SLTs, an analysis has been carried out where white Gaussian noise was

Class #

	1	2	3	4	5
1	94.97	2.90	1.10	1.03	0
2	0	97.63	0	0.07	2.30
3	0	0	94.10	4.33	1.57
4	0	1.10	1.80	90.87	6.23
5	0.87	0	0.83	1.43	96.87

Fig. 6: *Average Confusion Matrix using the Spectrogram Approach.*

Class #

	1	2	3	4	5
1	98.83	1.90	1.10	0.17	0
2	0	99.07	0	0.93	0
3	0	0	99.70	0	0.3
4	0	0.70	1.67	98.40	0.73
5	0.87	0.07	2.90	0.73	95.43

Fig. 7: *Average Confusion Matrix using the SLT Approach.*

added to raw I/Q data, assuming the original signal to be noiseless and injecting a noise level in order to have SNR ranging between -10 and 10 dBs. As in the previous analysis, the average performance is derived for both approaches and the results are presented in Figure 8. The plot shows how the SLTs based approach overcomes the Spectrogram one in the presence of noise for all SNR levels considered, in particular, the improvement ranges between the 4% at 10 dBs to 15% at 0 dBs of SNR.

V. COMPUTATIONAL COMPLEXITY

To assess the trade-off in terms of computational complexity between the proposed SLT-based approach and using spectrogram, an execution time analysis was conducted. Specifically, a random complex signal was generated with normal distribution and length of 2432 samples to match the duration of the signals used for the feature extraction. The signal was then transformed 1000 times using two SLT of different orders and a spectrogram using the window and DFT length described in Section IV. Using MATLAB on an Intel(R) Xeon(R) CPU E5-1607 v2 @ 3.00GHz, 16 GB PC, the average computation time for the SLT was 1.82 s and 3.16 s for $o = [1, 30]$ and $o = [5, 40]$ respectively and 4 ms for the spectrogram. This implies approximately 3 orders of magnitude higher average computational
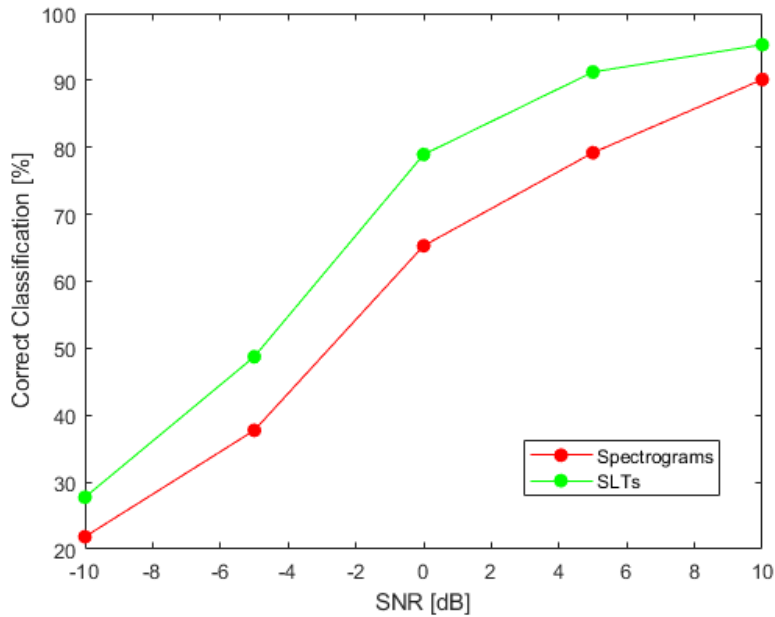
Fig. 8: *Average Correct Classification as a function of SNR for both approaches.*

time for the SLT compared to the spectrogram. Nevertheless, it should be noted that the spectrogram function is highly optimised in MATLAB compared to the STL.

VI. CONCLUSIONS AND FUTURE WORK

In conclusion, the Superlet approach introduced in this paper to compute mD signatures showed that it can help improve the performance in mD classification thanks to its super-resolution. The analysis of real data showed that using this higher resolution approach could benefit existing and future mD classification strategies. Of particular interest, indeed is the family of approaches using deep learning applied to the TFDs and that would have significant advantages if richer information is fed to the network [28], [29], [30].

ACKNOWLEDGMENT

REFERENCES

[1] V.C. Chen, F. Li, S. Ho, H. Wechsler. Micro-Doppler Effect in Radar: Phenomenon, Model, and Simulation Study. *IEEE Transactions on Aerospace and electronic systems*, vol. 42, no. 1, pp. 2–21, January 2006, doi: 10.1109/TAES.2006.1603402.

[2] V.C. Chen, D. Tahmoush, W.J. Miceli. In *Radar Micro-Doppler Signature Processing and applications*, The Institution of Engineering and Technology, 2014.

[3] V.C. Chen. The Micro-Doppler Effect of the Nonrigid Body Motion. In *The Micro-Doppler Effect in Radar*, 1st ed. Norwood, MA: Artech House, 2011, ch. 4, pp. 157–160.

[4] F. Fioranelli, M. Ritchie, S. Z. Gürbüz and H. Griffiths. Feature Diversity for Optimized Human Micro-Doppler Classification Using Multistatic Radar. In *IEEE Transactions on Aerospace and Electronic Systems*, vol. 53, no. 2, pp. 640-654, April 2017, doi: 10.1109/TAES.2017.2651678..

[5] S. Björklund, H. Petersson, G. Hendeby. Features for micro-Doppler based activity classification. *IET radar, sonar & navigation*, vol. 9, no. 9, pp. 1181–1187, December 2015, doi: 10.1049/iet-rsn.2015.0084.

[6] Y. Zhang, Y. Peng, J. Wang and P. Lei. Human Motion Recognition Based on Radar Micro-Doppler Features Using Bayesian Network. *2019 IEEE International Conference on Signal, Information and Data Processing (ICSIDP)*, 2019, pp. 1-5, doi: 10.1109/ICSIDP47821.2019.9173502.

[7] G.E. Smith, K. Woodbridge, C.J. Baker. Template based microdoppler signature classification. *2006 European Radar Conference*, 2006, pp. 158-161, doi: 10.1109/EURAD.2006.280298.

[8] G.E. Smith, K. Woodbridge, C.J. Baker. Micro-doppler signature classification. *2006 CIE International Conference on Radar*, 2006, pp. 1-4, doi: 10.1109/ICR.2006.343175.

[9] G.E. Smith, K. Woodbridge, C.J. Baker. Naive Bayesian radar microdoppler recognition. *2008 International Conference on Radar*, 2008, pp. 111-116, doi: 10.1109/RADAR.2008.4653901.

[10] A. Balleri, K. Chetty, K. Woodbridge. Classification of personnel targets by acoustic micro-Doppler signatures. *IET Radar, Sonar and Navigation*, pp. 943–951, 2011, doi: 10.1049/iet-rsn.2011.0087.

[11] C. Clemente, L. Pallotta, A. De Maio, J.J. Soraghan, A. Farina. A Novel Algorithm for Radar Classification Based on Doppler Characteristics Exploiting Orthogonal Pseudo-Zernike Polynomials. *IEEE Transactions on aerospace and electronic systems*, vol. 51, no. 1, pp. 417-430, January 2015, doi: 10.1109/TAES.2014.130762.

[12] G. Li, R. Zhang, M. Ritchie and H. Griffiths. Sparsity-Driven Micro-Doppler Feature Extraction for Dynamic Hand Gesture Recognition. *IEEE Transactions on Aerospace and Electronic Systems*, vol. 54, no. 2, pp. 655-665, April 2018, doi: 10.1109/TAES.2017.2761229.

[13] L. Yang, W. Zhang and W. Jiang. Ballistic Target Recognition based on Deep Learning by utilizing the micro-Doppler feature. *2022 IEEE 6th Advanced Information Technology, Electronic and Automation Control Conference (IAEAC)*, Beijing, China, 2022, pp. 1628-1632, doi: 10.1109/IAEAC54830.2022.9929850.

[14] Y. Ding, Y. Sun, G. Huang, R. Liu, X. Yu and X. Xu. Human Target Localization Using Doppler Through-Wall Radar Based on Micro-Doppler Frequency Estimation. *IEEE Sensors Journal*, vol. 20, no. 15, pp. 8778-8788, 1 Aug.1, 2020, doi: 10.1109/JSEN.2020.2983104.

[15] Y. Kim and T. Moon. Human Detection and Activity Classification Based on Micro-Doppler Signatures Using Deep Convolutional Neural Networks. *IEEE Geoscience and Remote Sensing Letters*, vol. 13, no. 1, pp. 8-12, Jan. 2016, doi: 10.1109/LGRS.2015.2491329.

[16] J.Zabalza, C. Clemente, G. Di Caterina, J. Ren, J.J. Soraghan, S. Marshall. Robust PCA for Micro-Doppler Classification using SVM on Embedded Systems. *IEEE Transactions on aerospace and electronic systems*, vol. 50, no. 3, pp. 2304-2310, July 2014, doi: 10.1109/TAES.2014.130082.

[17] S.S. Ram, H. Ling. Analysis of microDopplers from human gait using reassigned joint time-frequency transform. *Electronics Letters*, vol. 43, no. 23, pp. 1309-1311, 2007, doi: 10.1049/el:20071515.

[18] K. Abratkiewicz, P. Samczyński. Multitaper Time-Frequency Reassigned Spectrogram in Micro-Doppler Radar Signal Analysis. *2021 Signal Processing Symposium (SPSympo)*, LODZ, Poland, 2021, pp. 1-5, doi: 10.1109/SPSympo51155.2020.9593356.

[19] S. Liaqat, M. bin Ihsan, S. Z. Asghar, A. Ejaz, A. Javed. High resolution 2D time frequency representation of radar micro-Doppler pedestrian signal. *2013 European Radar Conference, Nuremberg, Germany, 2013, pp. 168-171*.

[20] V.V. Moca, H. Bârzan, A. Nagy-Dăbâcan, R.C. Mureșan. Time-frequency super-resolution with superlets. *Nature Communications*, no. 337, January 2021, doi: https://doi.org/10.1038/s41467-020-20539-9.

[21] S. Cheung, JS. Lim. Combined multiresolution (wide-band/narrow-band) spectrogram. *IEEE Transactions on Signal Processing*, vol. 40, no. 4, pp. 975-977, April 1992, doi: 10.1109/78.127970.

[22] P. Loughlin, J. Pitton, B. Hannaford. Approximating time-frequency density functions via optimal combinations of spectrograms. *IEEE Signal Processing Letters* , vol. 1, no. 12, pp. 199-202, December 1994, doi: 10.1109/97.338752.

[23] M. Farge, K. Schneider. Wavelets: Application to Turbulence. *Encyclopedia of Mathematical Physics, Academic Press*, pp. 408-420, 2006, doi: 10.1016/B0-12-512666-2/00274-1.

[24] H. Bârzan, V.V. Moca, A. Ichim, R.C. Mureșan. Fractional Superlets. *28th European Signal Processing Conference (EUSIPCO)*, 2020, doi: 10.23919/Eusipco47968.2020.9287873.

[25] R.L. Allen, D. Millis. Time-Frequency Signal Transforms. *Wiley-IEEE Press*, pp. 712–801, May 2004, doi: 10.1002/047166037X.ch10.

[26] RFbeam Microwave GmbH. Datasheet V-MD3 digital 3D radar transceiver. *Revision A: Initial Version*, May 2020.

[27] Y. Xu, R. Goodacre On Splitting Training and Validation Set: A Comparative Study of Cross-Validation, Bootstrap and Systematic Sampling for Estimating the Generalization Performance of Supervised Learning. *Journal of Analysis and Testing*, vol. 2, no. 3, pp. 1-14, October 2018, doi: 10.1007/s41664-018-0068-2.

[28] M. Czerkawski, C. Clemente, C. Michie, I. Andonovic and C. Tachtatzis. Robustness of Deep Neural Networks for Micro-Doppler Radar Classification. *23rd International Radar Symposium (IRS), Gdansk, Poland*, 2022, pp. 480-485, doi: 10.23919/IRS54158.2022.9905017.

[29] P. Addabbo, M.L. Bernardi, F. Biondi, M. Cimitile, C. Clemente, D. Orlando. Temporal Convolutional Neural Networks for Radar Micro-Doppler Based Gait Recognition. *Sensors 2021* 21, no. 2: 381, doi: 10.3390/s21020381

[30] M. Czerkawski, C. Ilioudis, C. Clemente, C. Michie, I. Andonovic and C. Tachtatzis. " A Novel Micro-Doppler Coherence Loss for Deep Learning Radar Applications. *2021 18th European Radar Conference (EuRAD)*, London, United Kingdom, 2022, pp. 305-308, doi: 10.23919/EuRAD50154.2022.9784491.